energies

MDPI

Article

Investigation of the Temperature Sensitivity of 20-Years Old Field-Aged Photovoltaic Panels Affected by Potential Induced Degradation

Oscar Kwame Segbefia * and Tor Oskar Sætre

Department of Engineering Sciences, University of Agder, 4879 Grimstad, Norway; tor.satre@uia.no
* Correspondence: oscar.k.segbefia@uia.no; Tel.: +47-4637-9399

Abstract: One effect of moisture ingress on solar panels is potential induced degradation (PID). Solar panels affected by PID experience large leakage currents between the solar cells and the module's frame, which leads to substantial power degradation. In the present work, the temperature coefficients of 3 old PV panels affected by PID were investigated. In the electroluminescence images, solar cells nearer to the edge of the modules appear darker due to ohmic shunting. IR thermal images acquired under clear sky outdoor conditions show that the majority of the warmer cells (hotspots) were located closer to the edge of the modules. The difference in cell temperature (ΔT) due to PID effect ranges from 7 °C to 15 °C for the 3 field-aged modules. The average temperature coefficient of efficiency ($\beta_{\eta m}$) was found to be −0.5%/°C. Also, it was observed that the temperature coefficients of open circuit voltage (β_{Voc} = −0.4%/°C), maximum power point voltage (β_{Vmpp} = −0.5%/°C), and fill factor (β_{FF} = −0.2%/°C), were the underlying factors for the degradation in the P_{max} of the old solar panels affected by PID. This accounted for an average 1.2%/year overall degradation in the efficiency of these modules. Most notably, it was discovered that the PV modules affected by PID show negative temperature coefficients of maximum power point current (β_{Jmpp}) due to large leakage currents. This observed negative β_{Jmpp} we believe is characteristic of PV panels affected by PID.

Keywords: potential induced degradation; shunting; temperature coefficient; leakage current; field-aged

check for updates

Citation: Segbefia, O.K.; Sætre, T.O. Investigation of the Temperature Sensitivity of 20-Years Old Field-Aged Photovoltaic Panels Affected by Potential Induced Degradation. *Energies* **2022**, *15*, 3865. https://doi.org/10.3390/en15113865

Academic Editors: Pedro Dinis Gaspar, Pedro Dinho da Silva and Luís C. Pires

Received: 20 April 2022
Accepted: 14 May 2022
Published: 24 May 2022

Publisher's Note: MDPI stays neutral with regard to jurisdictional claims in published maps and institutional affiliations.

Copyright: © 2022 by the authors. Licensee MDPI, Basel, Switzerland. This article is an open access article distributed under the terms and conditions of the Creative Commons Attribution (CC BY) license (https://creativecommons.org/licenses/by/4.0/).

1. Introduction

One of the underlying effects of moisture ingress on photovoltaic (PV) modules is potential induced degradation (PID) [1–7]. PID occurs when there is an increased material conductivity and leakage current between the PV module's frame and the cells [8–15]. This has severe consequences for PV module power reliability and can constitute up to 100% of power loss in PV plants [16].

According to Naumann et al. [10], high surface defect density on interdigitated back contact (IBC) solar cells results in decreased field effect passivation. Decreased field effect passivation leads to high surface recombination, and hence, causes PID of polarization/passivation (PID-p) type. However, PID-p is temporary and reversible [10,17–19]. Investigations revealed that the transport of mobile ions, especially sodium (Na+) ions, within the PV module bulk is responsible for the PID of shunting (PID-s) type [2,15,20,21]. High conductivity of sodium decorated stacking faults across the solar cell emitter leads to shunting, hence, PID-s [2,20]. PID-s manifests itself in the degradation in the open circuit voltage, short circuit current, and fill factor [2,3]. Hence, PID-s type appears to be the key problem in the field [17].

There have been efforts to prevent PID at the cell and module manufacturing levels, installation, and during operation [2,5,22]. Current-voltage (I-V) characterization, electroluminescence (EL), and infrared (IR) thermography could be used to detect and monitor the onset of PID in PV plants under sunlight or in the dark with external bias conditions [2,21]. PID-s cells are identified as warmer cells in IR thermal images and darker

cells in EL images [3,6,15]. According to Carolus et al. [14], Current-voltage (I-V) and external quantum efficiency (EQE) measurements could be used to differentiate PID-s from PID-p. Proposed methods for reversing the PID effect appears to be saddled with other limitations [8,22]. Indeed, the TS IEC 62804-1 standard exists to ensure PID reliability of commercial PV modules. However, the PID effect continues to be a challenge for the PV community [2,6,20,23,24].

In addition to power degradation, PID also induces mismatch losses due to non-uniform degradation [9,20,25,26]. Degraded cells that are affected by PID cause current reverse biasing, which leads to local overheating or joule heating [14,27]. This triggers hotspots, which influence the PV module operating temperature (T_m), hence, the temperature sensitivity [20,25,28]. According to Islam et al. [23], PID in polycrystalline solar panels can accelerate cell crack propagation and can lead to the degradation in the temperature coefficient of efficiency. In addition, Wang et al. [24] observed an increased temperature coefficient of maximum power (P_{max}) in PV modules affected by PID. Extensive research on the influence of the temperature sensitivity on PV modules main electrical parameters is available in literature [25,26,28–31]. However, studies on the influence of PID on the temperature coefficients of PV modules are rare [20,25,26,28]. Moreover, only a few were done on field-aged PV modules [23,24]. Yet, we have not found any report on the influence of PID on the temperature coefficients of the maximum power point voltage (β_{Vmpp}) and current (β_{Jmpp}) of PV modules.

A procedure for detecting PID based on temperature coefficient profiling of PID affected field-aged multicrystalline silicon (mc-Si) PV modules is presented in this contribution. I-V characterization, EL, and IR thermal imaging were used for the investigation. It turned out that PV modules affected by PID could be detected by monitoring the temperature coefficient of maximum power point current (β_{Jmpp}). Section 2 presents the material and methods used for the investigation and the results and the insights from the investigation are presented in Section 3.

2. Materials and Methods

In the present work, field-aged NESTE NP100G12 multicrystalline silicon (mc-Si) PV modules affected by PID were investigated. The 3 solar panels (namely A, B, and C) were chosen from a batch of solar panels which were installed on a Renewable Energy Park in Dømmesmoen, Grimstad (58.3447° N, 8.5949° E), Norway in the year 2000. However, the PV modules on the Energy Park were decommissioned in 2011 and were kept securely for research purposes [32]. In an earlier report on the types of defects and faults modes of these old solar panels by the present authors, EL and IR thermal data of PV panel C was used to show that some of the old PV panels were affected by PID. The manufacture's data sheet and the measured electrical data on the 3 old PV panels (namely A, B, and C) is summarized in Table 1.

Table 1. Technical data sheet (2000) and the measured electrical parameters (2021) of old solar panels normalized to Standard Test Conditions (STC).

PV Module		P_{max} (W)	V_{oc} (V)	I_{sc} (A)	V_{mpp} (V)	I_{mpp} (A)	*FF* (%)	η (%)
2000 (Data sheet)		100	21.6	6.7	16.7	6.0	70	13.0
2021	A	75.0	19.5	5.9	14.3	5.2	65	9.7
	B	75.9	19.3	6.1	14.2	5.3	65	9.9
	C	78.3	19.6	6.1	14.7	5.3	66	10.2

The PV modules were made using anodized aluminum (Al-) frame, low iron tempered front glass, ethylene vinyl acetate (EVA) encapsulation, white multi-layered Tedlar®/Polyester/Tedlar® (TPT) backsheet, and 2 weatherproof plastic casing junction boxes (accommodating a bypass diode each). Each PV module consists of (12 × 2) series connected solar cells and 3 substrings, refer to Figure 1. The solar cells feature a full area screen-printed Al-grid rear surface with dimensions of 100 × 100 mm^2 and a titania antireflective coating (ARC).

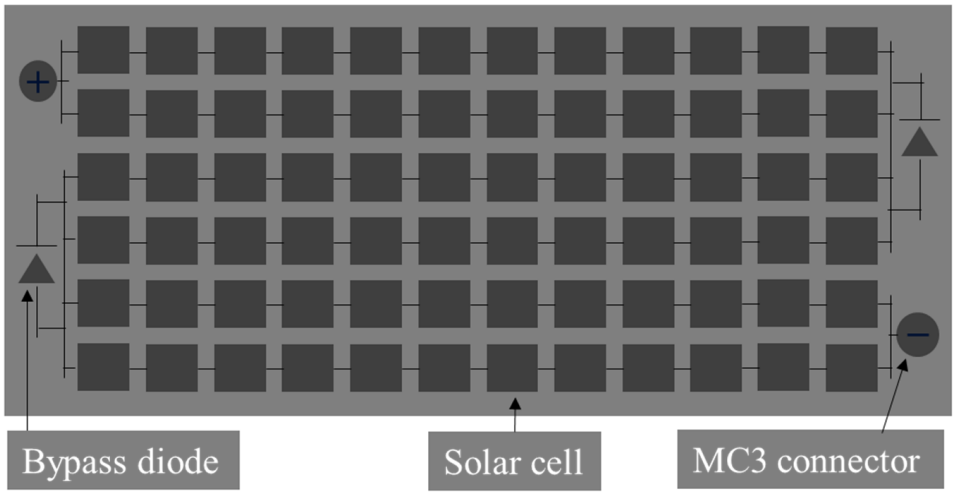

Figure 1. Electrical layout of the field-aged PV modules. Three serially circuited substrings; each consisting of a pair of 12 series connected solar cells in 3 series connected substrings.

2.1. I-V Measurements

The sampled old solar panels were each taken through electrical performance measurements using an HT® Instruments I-V 500 w I-V Curve Tracer. This was done by following the IEC 60904-1 standard. By these measurements, information on the maximum power (P_{max}), open circuit voltage (V_{oc}), maximum power point voltage (V_{mpp}), short circuit current (I_{sc}), maximum power point current (I_{mpp}), fill factor (FF), in-plane irradiance (G_I), and module temperature characteristics of each panel at Standard Test Conditions (STC) was acquired. STC indicates solar cell temperature at 25 °C, G_I at 1000 W/m^2 and air mass 1.5 (AM1. 5) spectrum for commercial solar PV panels. The entire experimental procedure was carried out under clear sky in-plane irradiance conditions (960–1060 W/m^2). The I-V tracer converted all measurements to STC automatically to minimize errors associated with data acquisition.

2.2. Temperature Coefficient Profiling

On a clear sky sunny day in the summer, the PV modules were taken out to the outdoor measuring rack in turns from a storeroom where the modules were kept. The PV module and the reference device were shaded using a cardboard. Measurement was initiated immediately after the shade was removed. The measurements on the 3 field-aged PV modules were done on the same day between 12.30 and 14.30 h and at wind speed less than 2 ms^{-1}. According to IEC 60891-4 standard, the temperature range of the data values should be at least 30 °C. However, this seems challenging in practical field measurements, especially for the investigation site.

A graph of electrical parameters (P_{max}, V_{oc}, I_{sc}, FF, η_m, V_{mpp}, I_{mpp}) versus PV module's temperature (T_m) was plotted and a least-squares-fit graph through each data set was acquired to get the relative temperature coefficients. The regression equation for such relation can be represented as $y = mx + c$, where m and c are the slope (temperature coefficient) and the intercept (the value of the electrical parameter at 0 °C), respectively [33]. The relative temperature coefficient of parameter X (β_x) in%/°C was calculated by dividing the slope of parameter X by the intercept of parameter X. That is, $\beta_x = m/c$.

2.3. Electroluminescence (EL) Tomography

EL tomography is interesting especially for characterizing old PV panels affected by PID. The 3 sampled PV panels were taken through the EL characterization in a dark room using the BrightSpot EL Test Kit, see Figure 2. The kit comprises of a 24 megapixels modified DSLR (digital single-lens reflex) Nikon D5600 camera, DC power supply set, and computer with data acquisition and image processing software. The image acquisition and processing were done

according to the IEC 60904-13 standard and the IEA procedure [3,15]. The EL characterization of the PV modules was done under $0.1I_{sc}$ and at I_{sc} current density conditions.

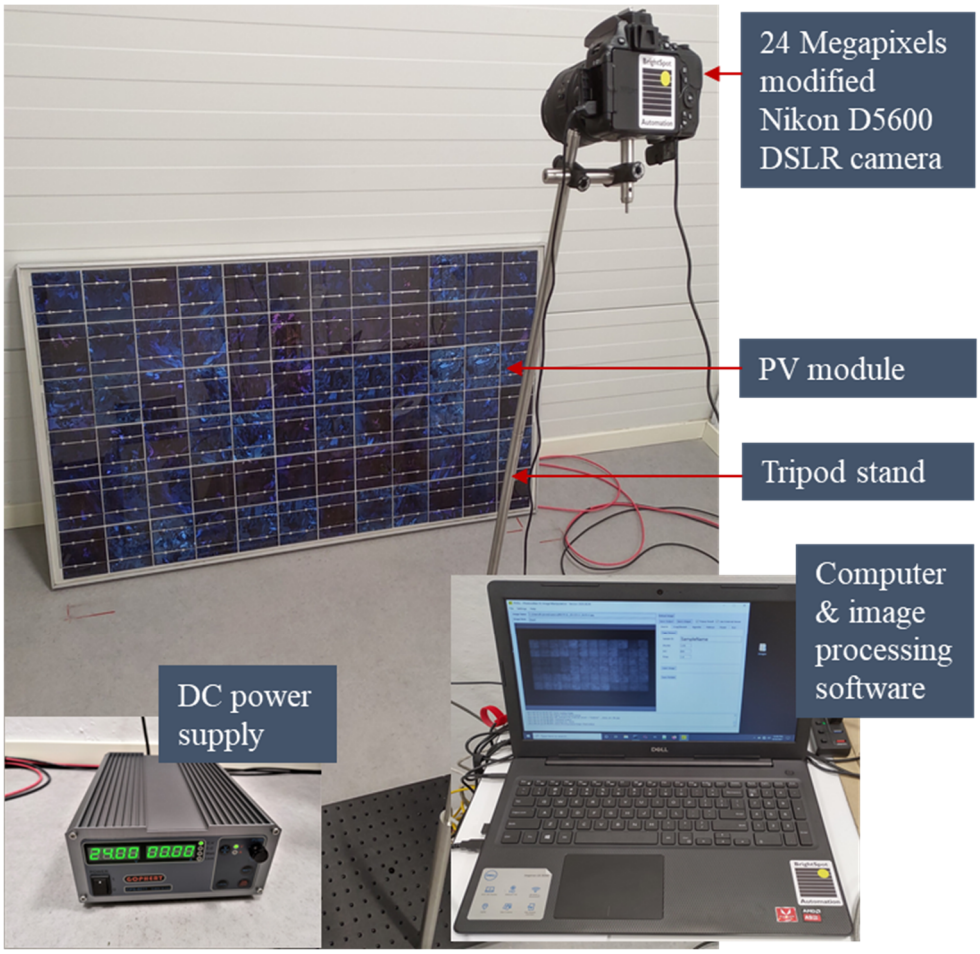

Figure 2. Experimental setup of the EL imaging system. The system runs on a DC power supply.

2.4. Infrared (IR) Thermal Imaging

The sampled solar panels were also taken through IR thermography using the Fluke Ti400 Infrared Camera ($\lambda \approx 650$ nm) as per the IEA recommended procedure [15] and the IEC 62446-3 standard. Figure 3 shows the outdoor experimental setup. Measurements were done under clear sky field conditions. The IR thermal images were acquired after soaking the PV modules in the sun for at least 15 min, as prescribed by the IEC 62446-3 standard.

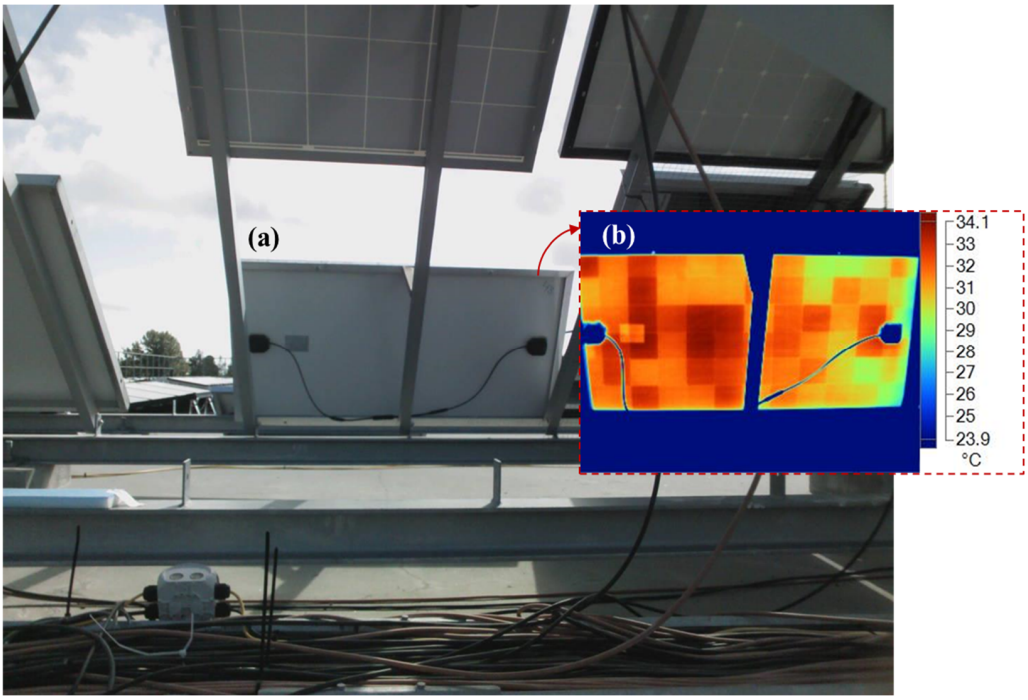

Figure 3. (**a**) Visual image and (**b**) IR thermal image (insert) of a PV module measured from the backside during the outdoor IR thermal imaging. The supporting metal trestle (behind the PV module) and the cables in the visual image show corresponding blue traces in the IR thermal image.

3. Results and Discussion

3.1. I-V Characteristics of the PV Panels

Figure 4 illustrates the I-V characteristics of the field-aged PV Modules A, B, and C. The I-V curve for the manufacturer's data sheet in 2000 illustrates the I-V characteristics of the panels when they were new, i.e., when they were not affected by PID. However, in 2021, when the solar panels were affected by PID, the 3 panels show similar degradation trend in electrical characteristics. There was ca. 10% degradation in both I_{sc} and V_{oc} and ca. 24% degradation in P_{max} over the 20 years. That is, annual degradation of ca. 0.5% in I_{sc} and V_{oc} and ca. 1.2% in P_{max}, which agrees with observation elsewhere [34]. This resulted in the decrease in fill factor (F) of ca. 0.3%/year and a drop in efficiency of ca. 1.2%/year, see Table 1. A drop in the P_{max}, I_{sc}, V_{oc}, and FF was also observed by other researchers [3,14,15,29].

It was reported that the effect of PID is more severe under lower irradiation conditions as compared to STC [3,16]. This means that PV modules deployed in the cold regions are more susceptible to the PID effect than those deployed in climates with high regular irradiance conditions. Low irradiance and shading conditions predispose PV modules to mismatch losses, hence, hotspots [33]. These hotspots can induce the onset of PID [16,20,35]. For the 3 field-aged PV modules, the average degradation in the V_{mpp} and I_{mpp} were 0.7% and 0.6% per year, respectively (refer to Table 1). Figure 5 illustrates the relative change (Δ) in the electrical parameters of the old solar panels affected by PID over the 20 years. The relative change (Δ) in the electrical parameters of the PID affected old solar panels was computed as the difference between the datasheet values (2000) and the values measured in the year 2021, a recommended procedure by Köntges et al. [17].

The position of the box indicates the percentage degradation, and the dots show the outliers. The degree of deviation of the electrical parameter from the mean value is indicated by the length of the box. The degradation in the electrical parameters of the 3 old solar panels follow a similar trend. P_{max} shows more than 20% degradation over the 20 years, refer to Table 1. It appears from Figure 5 that the underlying cause of the P_{max} degradation is the degradation in all electrical parameters, especially degradation in V_{oc}

and V_{mpp}. Yet, it is blurry as to the degree of contribution from each electrical parameter to the overall degradation in P_{max}.

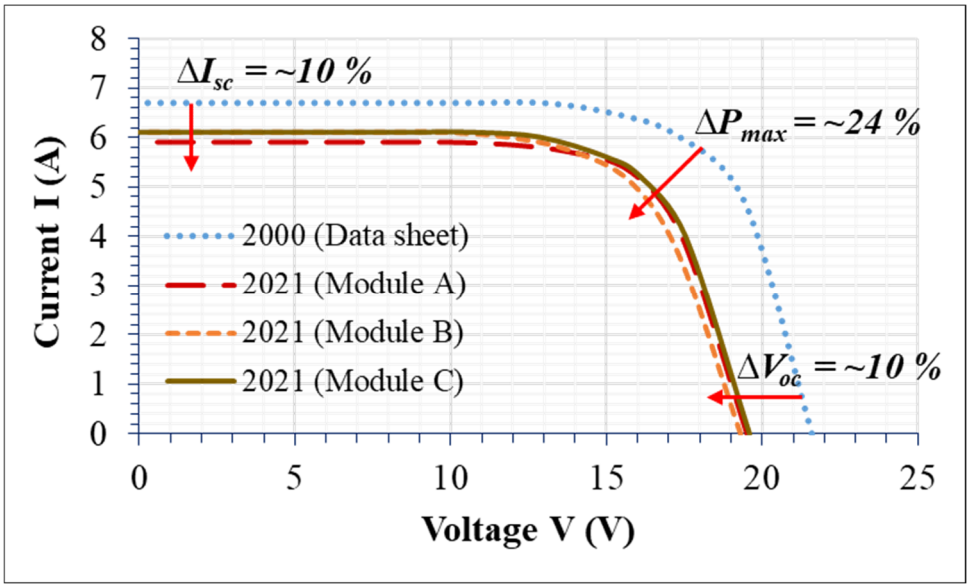

Figure 4. Normalized I-V characteristics of the 3 old PV panels (A, B, C). The data sheet curve by the manufacturer in the year 2000 is also shown.

It is known that P_{max} is directly related to the maximum power point voltage (V_{mpp}) and the maximum power point current (I_{mpp}) by the following relation:

$$P_{max} = V_{mpp} \cdot I_{mpp} \quad (1)$$

However, fill factor (FF) of a PV module could also be written as

$$FF = \frac{V_{mpp} \cdot I_{mpp}}{V_{oc} \cdot I_{sc}} \quad (2)$$

So, the maximum power output of a PV panel is related to the fill factor as

$$P_{max} = V_{oc} \cdot I_{sc} \cdot FF \quad (3)$$

The PV module efficiency (η_m) is related to the P_{max}, module's area (A_m), and the input power (P_{in}) as

$$\eta_m = \frac{P_{max}}{A_m \cdot P_{in}} \quad (4)$$

That means, any drop or degradation in V_{oc}, I_{sc}, FF, V_{mpp}, and I_{mpp} affects the P_{max} or η_m of the PV module directly, refer to Figure 4. Since the P_{in} for η_m calculations is assumed as 1 kWm^{-2}, $P_{max} \approx \eta_m / A_m$. A_m is the product of the solar cell's area and the number of solar cells in the module. From Table 2, the regression plots (which indicates the degree of correlation) for P_{max} versus V_{oc} and V_{mpp} gave $R^2 > 97$. On the other hand, the $R^2 < 0.6$ for I_{sc} and I_{mpp}. Resistance losses due to PID is the reason for the higher R^2 values for the fill factor (FF) of the modules, especially for solar panels A and C. The I-V curves of the modules in Figure 4 support this observation. Solar panel C appears to be the least affected by PID, hence, shows the weakest R^2 in both ΔI_{sc} and ΔI_{mpp}, refer to Table 2. This is because PID alters the current flow characteristics of the PV module [5,8,13]. When PID is caused by negative bias, it can induce optical degradation [5]. This is why most of these old solar panels were found to be affected by optical degradation as well.

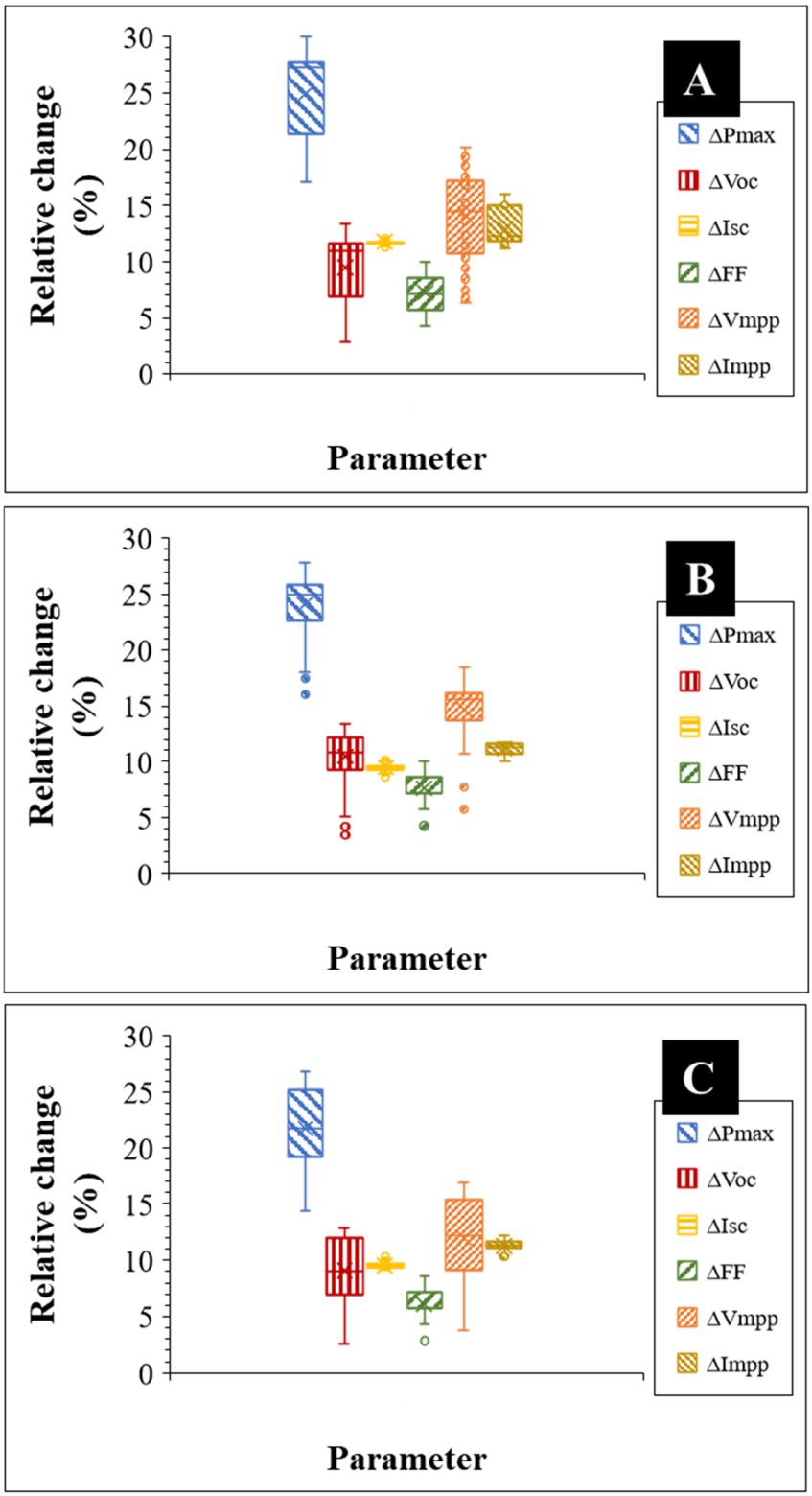

Figure 5. Degradation in the electrical parameters of the old PV panels under STC conditions using Box and Whisker plots. The tips of the boxes show the interquartile ranges. The internal lines show the median and the *x*-marks show mean. Δ is the difference between data sheet (2000) and measured (2021) values. Measurements were done under 960–1060 W/m^2 in-plane irradiance conditions.

Table 2. Correlation of the degradation in PV modules electrical parameters to the degradation in P_{max} due to PID. R^2 indicates the degree of correlation.

PV Module	R^2				
	ΔV_{oc}	ΔV_{mpp}	ΔFF	ΔI_{mpp}	ΔI_{sc}
A	0.98	0.99	0.86	0.23	0.47
B	0.98	0.98	0.57	0.55	0.17
C	0.99	0.99	0.88	0.06	0.04

Degradation in P_{max}, V_{oc}, V_{mpp}, and FF due to PID was also reported by other authors [3,14,16,29]. They believed that the loss in P_{max} due to PID could be up to 100% in severe cases [16]. The I-V characteristics of the old solar panels suggest that they are suffering from PID, as reported in other investigations [2,3,5,8,13,14,16,20,21,24,35].

3.2. Electroluminescence Characteristics

Figure 6 shows the EL analyses of the solar panels. The EL images were acquired under I_{sc} (Figure 6a–c) and $0.1I_{sc}$ (Figure 6d–f) forward bias conditions, respectively. The red marked out areas on the images in Figure 6 show some of the areas affected by PID in each PV module. In Figure 6a–c, apart from some darker spots, these images give little or no information on the areas affected by PID. This is because EL under I_{sc} conditions highlights metal contact or shunt issues [3,15]. In fact, contact issues such as cracks and corrosion are highlighted as darker spots in Figure 6a–c. Hence, EL under I_{sc} conditions are less suitable for detecting PID in PV modules, as observed in other studies [3,13,15].

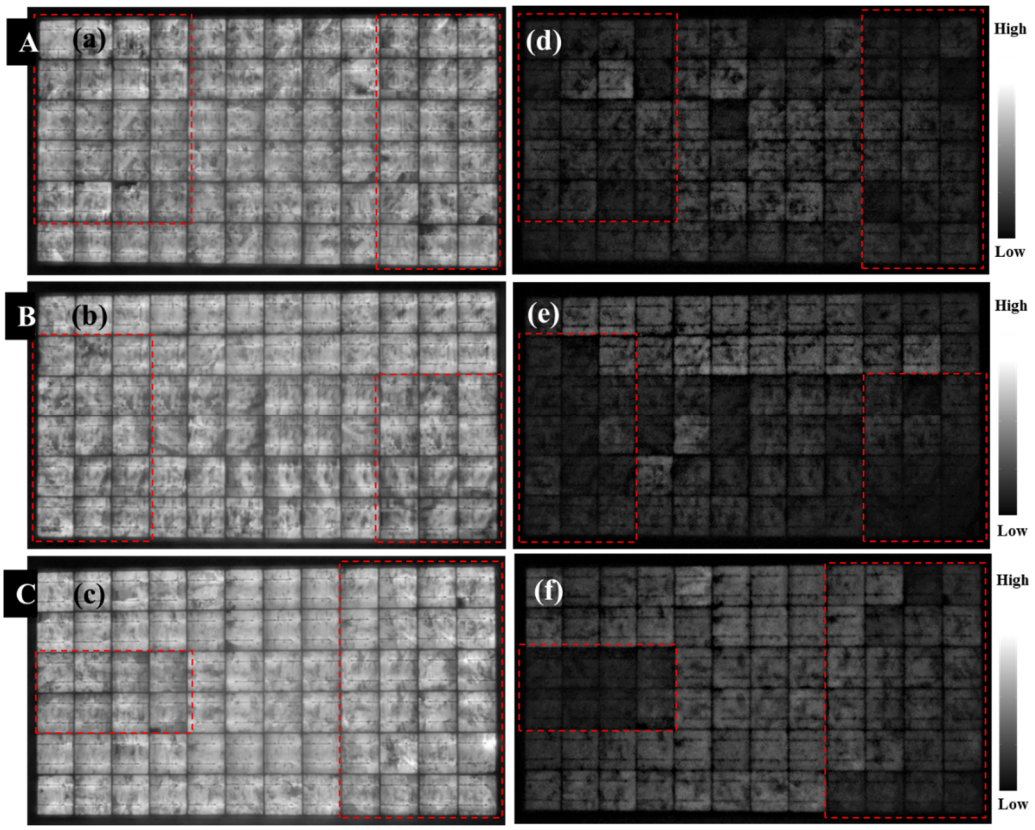

Figure 6. EL analyses of the 3 old solar panels under I_{sc} (**a–c**) and $0.1I_{sc}$ (**d–f**) conditions, respectively. Corresponding PID affected areas in EL images under both bias conditions are marked out in red. EL at $0.1I_{sc}$ revealed PID affected areas better.

On the other hand, under $0.1I_{sc}$ conditions, the effect of PID in the field-aged PV modules are well highlighted, see Figure 6d–f. The effect of PID manifests itself in the degradation of the solar cells located closer to the perimeter of the solar panel [8,22]. This accelerated degradation of the cells nearer to the frame of the PV module is due to high leakage currents associated with the PID effect [2,7,24]. Degraded solar cells appear as darker cells in the EL analyses due to strong ohmic shunting of the cell with the panel's Al-frame [24,27].

The PID affected areas in the solar panels are marked out in red. The trend in Figure 6 is that majority of the darker cells are located close to the edge of the old solar panels. The degradation pattern in Figure 6 suggests that these PV modules are affected by PID, as reported by other authors [3,9,14,15,35].

3.3. IR Thermal Image Characteristics

In IR thermal images, solar cells affected by PID appear as warmer cells or hotspots [16,36]. Figure 7 shows the IR thermograms of the 3 old solar panels (A, B, and C). In Figure 7, the areas marked out in white corresponds to the areas marked out in Figure 6. They show some of the areas in the PV modules that have been affected by PID. Figure 7 shows that majority of the warmer cells are located nearer to the perimeter of the old solar panels, as observed elsewhere [3,15,20,35].

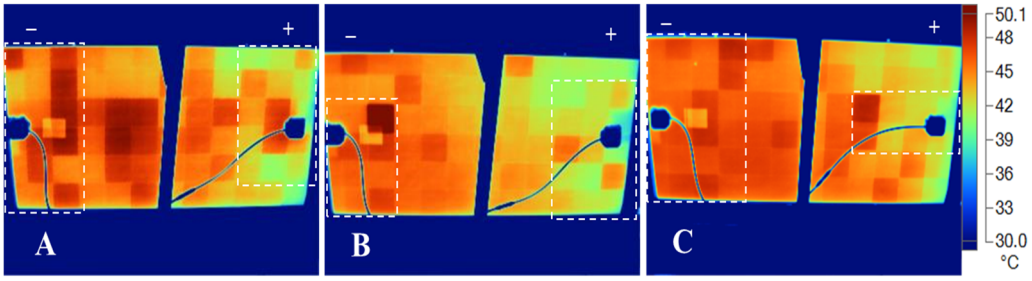

Figure 7. IR thermograms of the 3 old solar panels (**A**–**C**) affected by PID under clear sky outdoor conditions. Corresponding defects areas in Figure 6 are marked in white. The negative terminal (**left**) and the positive terminal (**right**) are indicated above the modules.

It could be seen that the locations of the warmer cells in the IR thermal images (Figure 7) correspond with the locations of the darker cells in the EL images, refer to Figure 6. Another observation from Figure 7 is that the cells which are closer to the negative terminal (left) of the field-aged PV modules are warmer than the cells which are located nearer to the positive terminal (right), especially those cells that are closer to the Al- frame. This was also reported by other researchers [9,15,35]. This is due to the direction of current flow in a PV module under illumination. Under in-plane radiation, current move by diffusion from the negative to the positive terminal. In PID affected areas, there is high resistance to current flow culminating into high module temperature localized to these areas [20,26,28], as observed in Figure 7.

This is opposite to the direction of current flow when the IR thermal imaging is done under forward bias (drift) conditions, as it is done in EL imaging. This also explains why the defective solar cells are clearly seen at the areas closer to the negative terminal in the field-aged PV modules. Also, high negative leakage current accelerates PID degradation [5,9,20,24,35]. Table 3 shows the extracted solar cells' temperatures of the old solar panels from the IR thermograms. The difference in the solar cells' temperature (ΔT) extracted from the IR thermograms of each solar panel was calculated according to Equation (4):

$$\Delta T = T_{cH} - T_{cL}, \quad (5)$$

where T_{cH} is the solar cell with the highest temperature and T_{cL} is the solar cell with the lowest temperature. ΔT due to PID for the 3 modules which have been affected by PID

ranges from 7 °C to 15 °C. Our results for these old panels agrees with the ΔT values reported in literature [15]. The reported ΔT values for solar panels affected by PID is in the range of ca. 7.5–30 °C depending on the severity of the PID effect [3,15,16].

Table 3. Difference in temperature (ΔT) of the solar cells with the highest temperature (T_{cH}) and lowest temperature (T_{cL}) for PV Modules A, B, and C which were affected by PID.

PV Module	Temperature (°C)		ΔT (°C)
	T_{cH}	T_{cL}	
A	36.9	29.5	7.4
B	51.3	36.7	14.6
C	49.5	40.5	9.0

The severity of the PID effect depends on the module materials- antireflection coating and encapsulation [6,21], module configuration [3,11], climatic conditions such as temperature and humidity [4,24,26], and voltage stress [5,9].

3.4. Temperature Coefficient Characteristics

Figure 8 illustrates the characteristics of the relative temperature coefficients of P_{max} (β_{Pmax}), V_{oc} (β_{Voc}), I_{sc} (β_{Jsc}), FF (β_{FF}), V_{mpp} (β_{Vmpp}), and I_{mpp} (β_{Jmpp}) of solar panels A, B, and C. Figure 8 compares the variation of each electrical parameter from the average value measured in the year 2021. Degradation in electrical parameters stems from the degradation in the relative temperature coefficients of PV modules [25,26,29]. That is, PID increases recombination in the emitter region of the solar cell [10,11,17–19], and this leads to a drop in the V_{oc} [25]. A drop in the V_{oc} influence the temperature characteristics of the solar panel [30,37]. A change in the V_{oc} accounts for more than 80% of the temperature sensitivity of the PV modules [25]. From Figure 8, the main root causes for the observed degradation in P_{max} became clearer, unlike in Figure 5. That is, the β_{Voc} and β_{Vmpp} of the PV modules are the main underlying causes of the P_{max} degradation.

Figure 8 also suggests that degradation in β_{FF} is significantly responsible for the degradation in P_{max}. This supports the earlier observation in Figure 5 that the solar panels affected by PID experience large resistance losses. Degradation in β_{Voc} and β_{FF} due to PID effects were reported earlier [20,26,28]. Figure 8 also shows clear outliers for β_{Pmax}, β_{Voc}, β_{Vmpp}, and β_{FF}. It could be seen that the majority of these outliers are correlated to higher temperature coefficient values which results from higher T_m [38]. This suggests that when T_m increases, the reliability of PV modules affected by PID decreases, as observed elsewhere [24,39].

Conceptually, the effect of T_m on P_{max} could be derived from Equation (3) because PV module parameters (V_{oc}, I_{sc}, FF) depend strongly on T_m [30,32,40]. Hence, could be represented as

$$\beta_{Pmax} = \beta_{Voc} + \beta_{Jsc} + \beta_{FF} \quad (6)$$

Interestingly, each of these parameters in Equation (5) depends on different loss mechanisms in the PV module [25,35]. These loss mechanisms mainly depend on the effects of different defects and fault mechanisms on the charge carrier generation-recombination balances at maximum power point (MPP) [35,41]. Therefore, Equations (1) and (5) could be represented in terms of V_{mpp} and I_{mpp} as

$$\beta_{Pmax} = \beta_{Vmpp} + \beta_{Jmpp} \quad (7)$$

The V_{oc} is the charge carrier generation-recombination characteristic of a solar panel. So, the temperature sensitivity of a solar panel improves when the V_{oc} increases [40,42]. Moreover, the β_{Voc} of a PV module accounts for 80–90% of the β_{Pmax} of the PV module [25]. For that matter, and inferring from Equation (6), β_{Vmpp} could be assumed to have the greatest impact on the degradation in β_{Pmax}, and hence, on P_{max} degradation. The corre-

lation of values of β_{Voc} and β_{Vmpp} to β_{Pmax} degradation is shown in Figure 9. In Figure 9, the regression plots show high correlation of $R^2 > 90$ and $R^2 > 88$ for β_{Voc} and β_{Vmpp}, respectively. Indeed, Figures 8 and 9 suggest that the root causes of degradation in the PV modules affected by PID are more accurately profiled using their temperature coefficients. They suggest that the β_{Voc} and β_{Vmpp} are the underlying factors for the degradation in the efficiency of the solar panels.

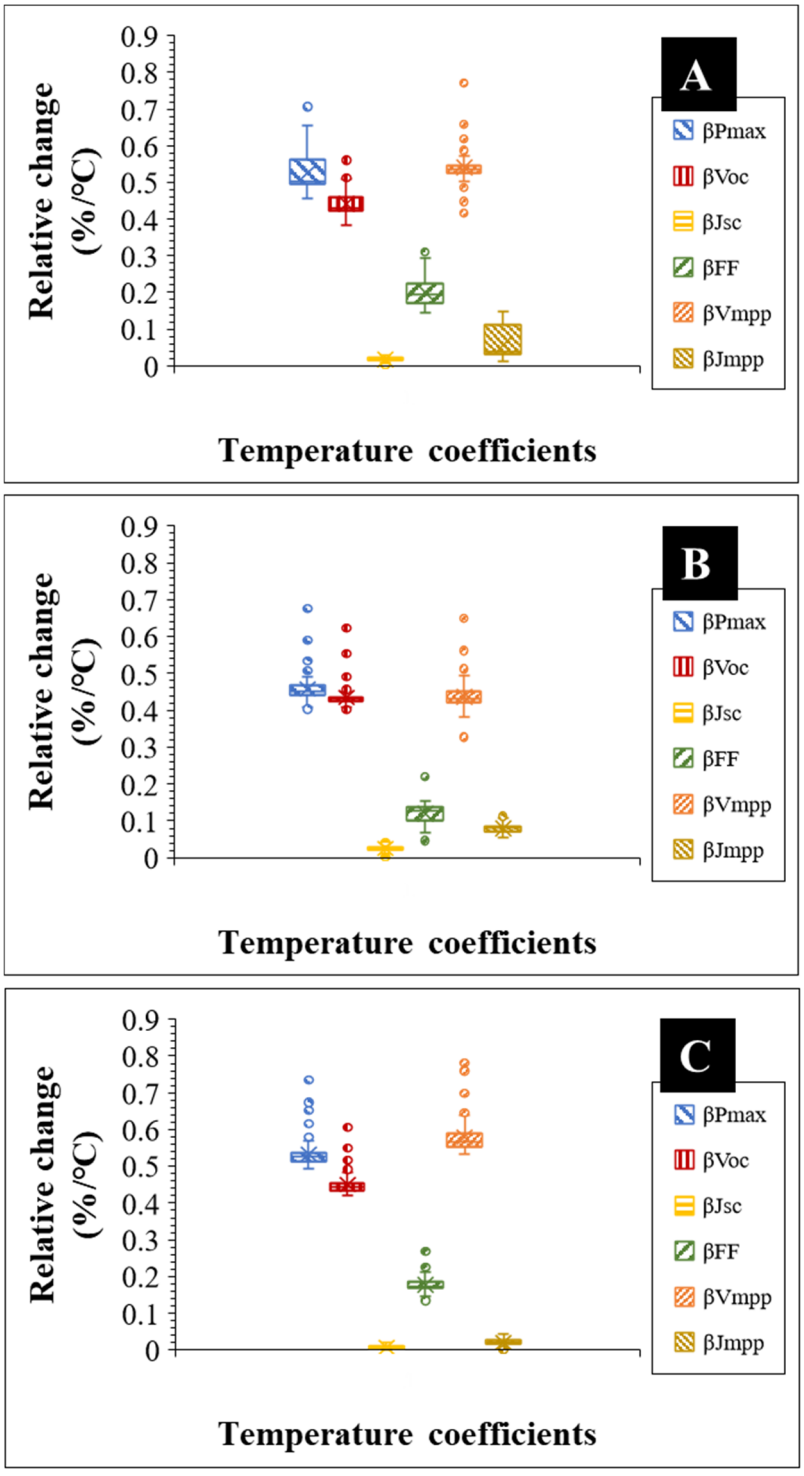

Figure 8. Change in the relative temperature coefficients of the 3 solar panels under STC conditions. The tips of the boxes show the interquartile ranges. The internal lines show the median and the *x*-marks show the mean. Measurements were done under 960 W/m^2–1060 W/m^2 in-plane irradiance conditions.

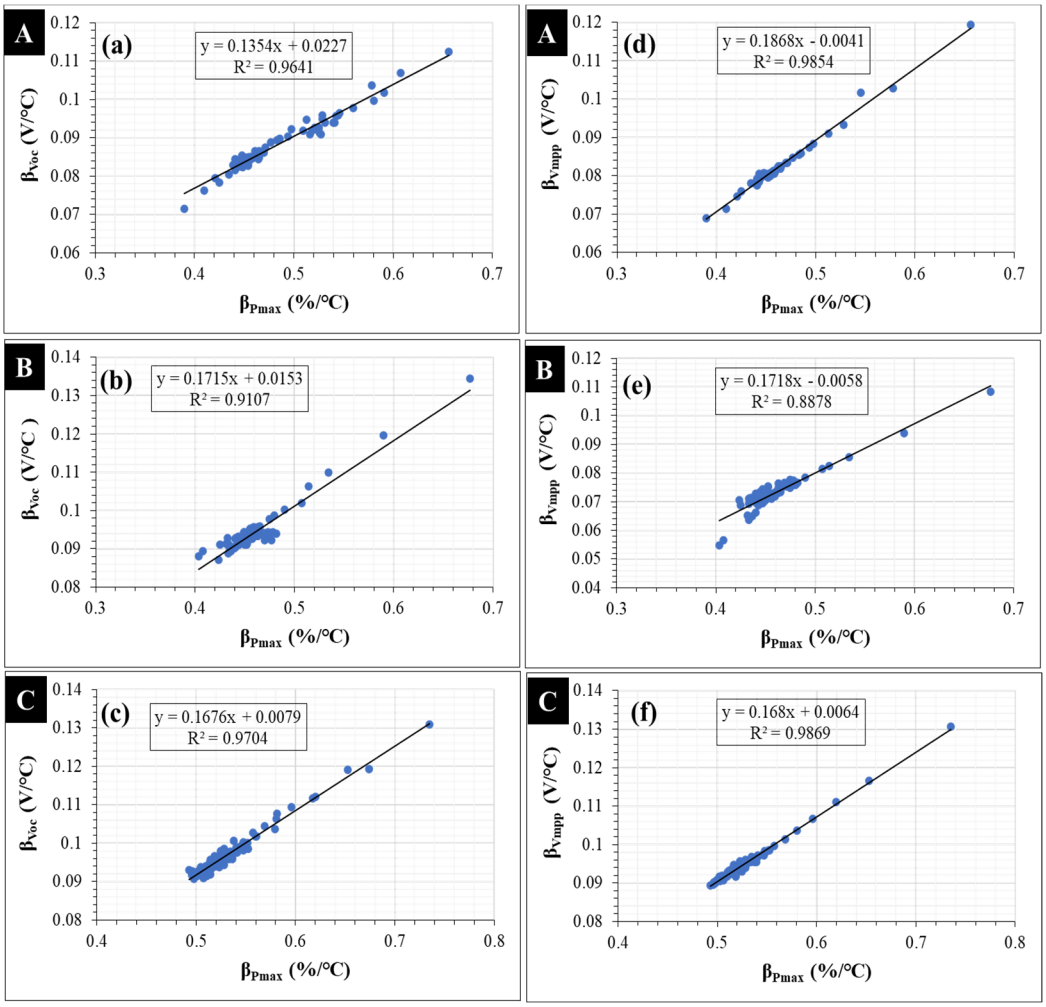

Figure 9. Dependence of absolute β_{Pmax} on absolute β_{Voc} (**a**–**c**) and β_{Vmpp} (**d**–**f**) of the 3 solar panels affected by PID. R^2 indicates the degree of correlation.

In Figure 9a,d, the slopes of the regression plots for PV Module A are 0.14 and 0.19 for β_{Voc} and β_{Vmpp}, respectively. However, the average of the slope values of β_{Voc} and β_{Vmpp} is ca. 0.17. Interestingly, from Figure 9, the slopes of PV Modules B and C for both β_{Voc} and β_{Vmpp} regression plots are ca. 0.17. Also, the slopes of the regression plots for β_{Vmpp} are closer to the average 0.17 value. Hence, we can predict the behaviour of β_{Pmax} better with the slopes of β_{Vmpp} for the PV modules affected by PID. This suggests that a unit change in β_{Pmax} is accounted for by 0.17 change in either β_{Voc} or β_{Vmpp} for each PV module affected by PID. The values of the slopes from the regression plots of β_{Pmax} versus β_{Voc} and β_{Vmpp} can be used to monitor PID severity in solar panels. On that basis, Figure 9 suggest that the effect of PID on PV Module A is the severest. Another observation from Figure 9d–f is that, when β_{Pmax} is zero, then by extrapolation, β_{Vmpp} will be ca. 0.4%/°C, 0.6%/°C, and 0.6%/°C for PV Module A, B, and C, respectively. These values are very close to the β_{Vmpp} values for the 3 field-aged PV modules in Table 4.

Table 4. Average temperature coefficients of the 3 solar panels.

PV Module	Temperature Coefficient (%/°C)					
	β_{Voc}	β_{Jsc}	β_{FF}	$\beta_{\eta m}$	β_{Vmpp}	β_{Jmpp}
A	−0.4	0.02	−0.2	−0.5	−0.5	**−0.06**
B	−0.4	0.03	−0.1	−0.5	−0.4	**−0.09**
C	−0.4	0.01	−0.2	−0.5	−0.5	**−0.02**

Figure 10 shows the profiles of the temperature coefficients of efficiency, η_m ($\beta_{\eta m}$) of the 3 solar panels. The average of $\beta_{\eta m}$ has been found to be ca. −0.5%/°C for the 3 field-aged PV modules. In literature, the $\beta_{\eta m}$ for mc-Si PV modules is 0.4%/°C [25,26,28–30]. PV modules in good conditions are expected to be more efficient when PV module operating temperature (T_m) drops below 25 °C [30,32]. However, by extrapolation when T_m is equal to zero, η_m < 13%, refer to Figure 10. This is characteristic of degraded PV modules which are suffering from resistive losses [20,26,40].

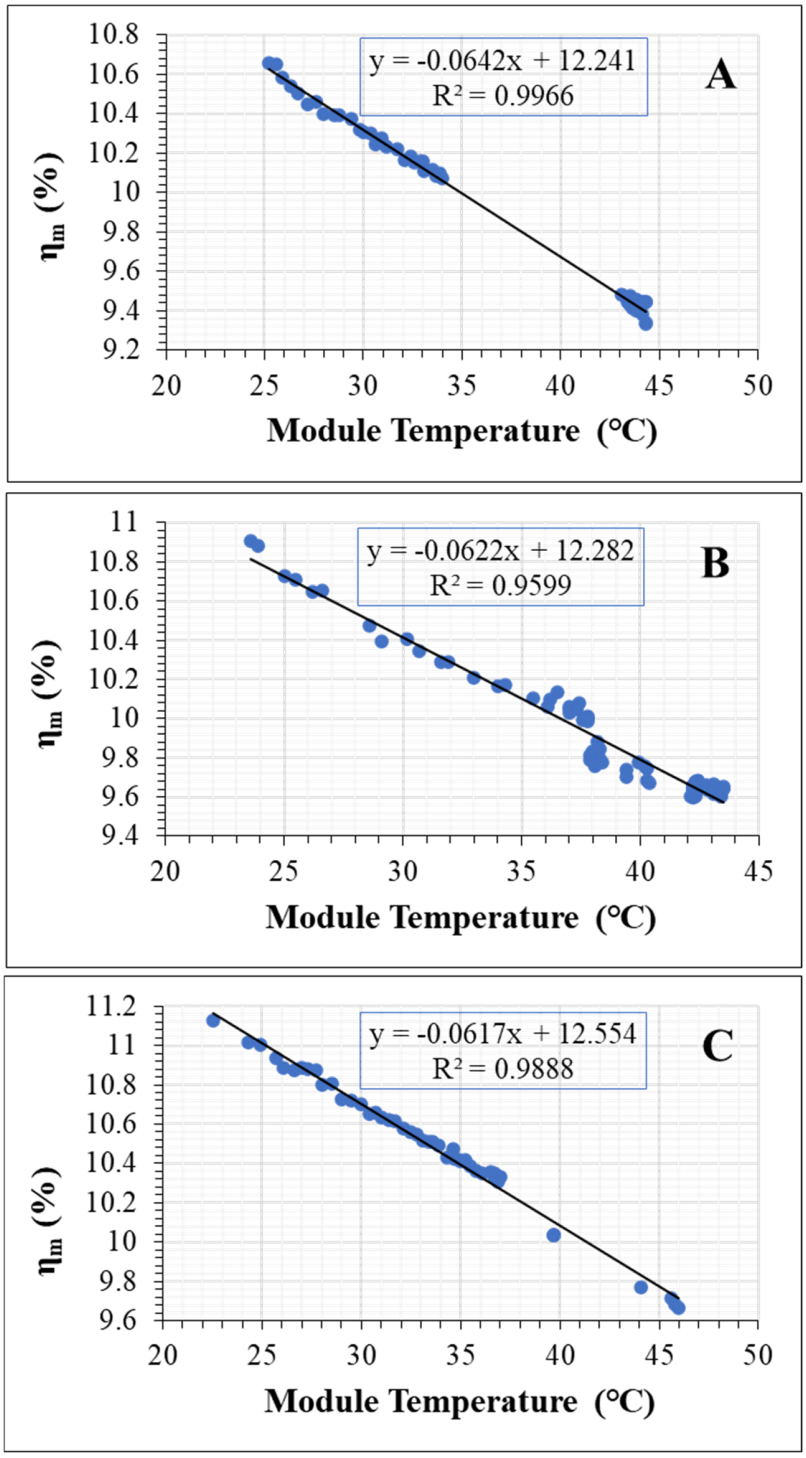

Figure 10. The relationship among the efficiency (η_m), module temperature, and temperature coefficient of efficiency($\beta_{\eta m}$) of the 3 solar panels. R^2 indicates the degree of correlation.

The average temperature coefficients of the 3 solar panels are shown in Table 4. The observed values for β_{Voc} and β_{Vmpp} agree with the values reported by King et al. [30] for conventional mc-Si PV modules. However, the β_{Voc} values are far less than the $-1.2\%/^{\circ}C$ reported by Cheng et al. [38] and the $-0.7\%/^{\circ}C$ reported by Wang et al. [24] for PV modules affected by PID. On the other hand, the β_{Jsc} values are relatively lower for these PV modules that have been affected by PID than observed elsewhere [24,38]. This suggests that in solar panels affected by PID, the contribution from thermally generated electrons towards the overall current density is less.

In addition, the β_{FF} values for the 3 field-aged PV modules are lower than the $-0.4\%/^{\circ}C$ reported for β_{FF} by Cheng et al. [38] for solar panels affected by PID. The fact that the modules studied by Cheng et al. [38] were aged artificially whiles our modules were field aged should not be ignored. Comparison of lab and field results are to be done with caution due to factors of uncertainty [43,44]. Our values are also in a good agreement with the $-0.2\%/^{\circ}C$ reported for β_{FF} by Wang et al. [24] for solar panels affected by PID.

Interestingly, the β_{Jmpp} of all the 3 solar panels show negative values. It is believed that the negative β_{Jmpp} values observed for the 3 old solar panels is due to the large leakage current experienced by PV modules affected by PID. Indeed, earlier investigation on the temperature profiles of solar panels affected by optical degradation indicated that negative β_{Jmpp} values are likely when the electrical circuit of the module is affected. However, in such cases, the β_{Jmpp} values are relatively higher and the β_{Jsc} values are by far higher as well. In that investigation, one of the modules affected by optical degradation showed a β_{Jmpp} of $-0.01\%/^{\circ}C$ and an average β_{Jsc} for the 3 modules was $0.05\%/^{\circ}C$. Moreover, a majority of the darker cells in the EL and warmer cells in IR thermal images were closer to the edge of the PV module affected by optical degradation. This suggests that the module in question is affected by at least optical degradation and PID. It is known that PID can lead to optical degradation and vice versa [5].

Furthermore, an earlier investigation on some of the solar panels under partial shading conditions, negative β_{Jmpp} values were observed for the modules investigated. However, under partial shading conditions, beside the peculiar I-V characteristics, the degradation in the P_{max} strongly depends mainly on the degradation in the β_{Jmpp} and β_{FF}. Moreover, under partial shading conditions, the effect on $\beta_{\eta m}$ becomes far higher, with $\beta_{\eta m} \geq -0.6\%/^{\circ}C$ [33]. It therefore suggests that an effective, quick, and reliable method of detecting PID in solar panels is to monitor the temperature coefficients, and specifically, the β_{Jmpp} of PV panels.

4. Conclusions

The temperature coefficients of 20 years old field-aged mc-Si PV modules which were affected by PID were investigated. Characterization utilized I-V characterization, EL imaging, IR thermal imaging, and temperature coefficient profiling. The results showed that the field-aged PV modules were indeed affected by PID. EL images acquired under $0.1I_{sc}$ indoor conditions show degraded darker cells located closer to the perimeter of the PV modules. The weak signal of the cells closer to the edge of the modules is due to strong ohmic shunting of the solar cells with the PV module's Al- frame. In the IR thermal images acquired under clear sky conditions, majority of the warmer cells (hotspots) were seen closer to the perimeter of the modules. In addition, areas closer to the negative terminals were also observed to be warmer than areas closer to the positive terminals. Our results show that the module ΔT due to PID ranges from 7 °C to 15 °C for the 3 old solar panels.

The modules show an average degradation of 0.5%/year in both I_{sc} and V_{oc}, 1.2%/year in P_{max}, and 0.3%/year in fill factor. For the 3 field-aged PV panels, the average degradation in the V_{mpp} and I_{mpp} were 0.7% and 0.6% per year, respectively. It turns out that the key underlying causes for PID in the field-aged PV modules and the subsequent degradation is degradation in V_{oc}, V_{mpp}, and FF. The average temperature coefficients of $\beta_{\eta m}$, β_{Voc}, β_{Jsc}, β_{FF}, β_{Jmpp}, and β_{Vmpp} were found to be $-0.5\%/^{\circ}C$, $-0.4\%/^{\circ}C$, $0.02\%/^{\circ}C$, $-0.2\%/^{\circ}C$, $-0.06\%/^{\circ}C$, and $-0.5\%/^{\circ}C$, respectively. This shows that all the temperature coefficients of the field-aged modules have undergone some form of degradation. However, it was

observed that the β_{Voc}, β_{Vmpp}, and β_{FF} were the primary factors for the degradation in the P_{max} for the old solar PV panels affected by PID. This translated into an average 1.2%/year overall degradation in the efficiency of these modules.

Most interestingly, it was observed that solar panels affected by PID show negative β_{Jmpp} due to large leakage currents. Hence, PID could be detected decisively by monitoring the β_{Jmpp} of solar PV panels. These findings have the potential of enhancing the existing knowledge on defects and faults diagnostics in PV arrays.

Author Contributions: Conceptualization, O.K.S.; methodology, O.K.S.; validation, O.K.S.; investigation, O.K.S.; resources, T.O.S.; writing—original draft preparation, O.K.S.; writing—review and editing, T.O.S.; supervision, T.O.S.; funding acquisition, T.O.S. All authors have read and agreed to the published version of the manuscript.

Funding: This research was funded by the University of Agder, Norway.

Institutional Review Board Statement: Not applicable.

Informed Consent Statement: Not applicable.

Data Availability Statement: The data presented in this study are available on request from the corresponding author. The data are not publicly available at this time as the data also forms part of an ongoing study.

Acknowledgments: The authors acknowledge the continuous support of the University of Agder, Norway.

Conflicts of Interest: The authors declare no conflict of interest.

References

1. Segbefia, O.K.; Imenes, A.G.; Saetre, T.O. Moisture ingress in photovoltaic modules: A review. *Sol. Energy* **2021**, *224*, 889–906. [CrossRef]
2. Luo, W.; Khoo, Y.S.; Hacke, P.; Naumann, V.; Lausch, D.; Harvey, S.P.; Singh, J.P.; Chai, J.; Wang, Y.; Aberle, A.G.; et al. Potential-induced degradation in photovoltaic modules: A critical review. *Energy Environ. Sci.* **2017**, *10*, 43–68. [CrossRef]
3. Köntges, M.; Kurtz, S.; Packard, C.; Jahn, U.; Berger, K.A.; Kato, K. *Performance and Reliability of Photovoltaic Systems: Subtask 3.2: Review of Failures of Photovoltaic Modules: IEA PVPS Task 13: External Final Report IEA-PVPS*; International Energy Agency, Photovoltaic Power Systems Programme: Paris, France, 2014.
4. Hoffmann, S.; Koehl, M. Effect of humidity and temperature on the potential-induced degradation. *Prog. Photovolt.* **2014**, *22*, 173–179. [CrossRef]
5. Hacke, P.; Terwilliger, K.; Smith, R.; Glick, S.; Pankow, J.; Kempe, M.; Bennett, S.K.I.; Kloos, M. System voltage potential-induced degradation mechanisms in PV modules and methods for test. In Proceedings of the 2011 37th IEEE Photovoltaic Specialists Conference, Seattle, WA, USA, 19–24 June 2011; pp. 000814–000820.
6. Virtuani, A.; Annigoni, E.; Ballif, C. One-type-fits-all-systems: Strategies for preventing potential-induced degradation in crystalline silicon solar photovoltaic modules. *Prog. Photovolt.* **2019**, *27*, 13–21. [CrossRef]
7. Lausch, D.; Naumann, V.; Breitenstein, O.; Bauer, J.; Graff, A.; Bagdahn, J.; Hagendorf, C. Potential-Induced Degradation (PID): Introduction of a Novel Test Approach and Explanation of Increased Depletion Region Recombination. *IEEE J. Photovolt.* **2014**, *4*, 834–840. [CrossRef]
8. Pingel, S.; Frank, O.; Winkler, M.; Daryan, S.; Geipel, T.; Hoehne, H.; Berghold, J. Potential induced degradation of solar cells and panels. In Proceedings of the 2010 35th IEEE Photovoltaic Specialists Conference, Honolulu, HI, USA, 20–25 June 2010; pp. 002817–002822.
9. Hylský, J.; Strachala, D.; Vyroubal, P.; Čudek, P.; Vaněk, J.; Vanýsek, P. Effect of negative potential on the extent of PID degradation in photovoltaic power plant in a real operation mode. *Microelectron. Reliab.* **2018**, *85*, 12–18. [CrossRef]
10. Naumann, V.; Geppert, T.; Grosser, S.; Wichmann, D.; Krokoszinski, H.J.; Werner, M.; Hagendorf, C. Potential-induced degradation at interdigitated back contact solar cells. In Proceedings of the 4th International Conference on Crystalline Silicon Photovoltaics (Siliconpv 2014), 's-Hertogenbosch, The Netherlands, 25–27 March 2014; Volume 55, pp. 498–503.
11. Yamaguchi, S.; Yamamoto, C.; Ohshita, Y.; Ohdaira, K.; Masuda, A. Influence of emitter position of silicon heterojunction photovoltaic solar cell modules on their potential-induced degradation behaviors. *Sol. Energy Mater. Sol. Cells* **2020**, *216*, 110716. [CrossRef]
12. Schütze, M.; Junghänel, M.; Koentopp, M.B.; Cwikla, S.; Friedrich, S.; Müller, J.W.; Wawer, P. Laboratory study of potential induced degradation of silicon photovoltaic modules. In Proceedings of the 2011 37th IEEE Photovoltaic Specialists Conference, Seattle, WA, USA, 19–24 June 2011; pp. 000821–000826.

13. Kwembur, I.M.; McCleland, J.L.C.; van Dyk, E.E.; Vorster, F.J. Detection of Potential Induced Degradation in mono and multi-crystalline silicon photovoltaic modules. *Phys. B—Condens. Matter* **2020**, *581*, 411938. [CrossRef]
14. Carolus, J.; Tsanakas, J.A.; van der Heide, A.; Voroshazi, E.; de Ceuninck, W.; Daenen, M. Physics of potential-induced degradation in bifacial p-PERC solar cells. *Sol. Energy Mater. Sol. Cells* **2019**, *200*, 109950. [CrossRef]
15. Jahn, U.; Herz, M.; Köntges, M.; Parlevliet, D.; Paggi, M.; Tsanakas, I. *Review on Infrared and Electroluminescence Imaging for PV Field Applications: International Energy Agency Photovoltaic Power Systems Programme: IEA PVPS Task 13, Subtask 3.3: Report IEA-PVPS T13-12*; International Energy Agency: Paris, France, 2018.
16. Tsanakas, J.A.; Ha, L.; Buerhop, C. Faults and infrared thermographic diagnosis in operating c-Si photovoltaic modules: A review of research and future challenges. *Renew. Sustain. Energy Rev.* **2016**, *62*, 695–709. [CrossRef]
17. Köntges, M.; Oreski, G.; Jahn, U.; Herz, M.; Hacke, P.; Weiß, K.-A. *Assessment of Photovoltaic Module Failures in the Field: International Energy Agency Photovoltaic Power Systems Programme: IEA PVPS Task 13, Subtask 3: Report IEA-PVPS T13-09*; International Energy Agency: Paris, France, 2017.
18. Halm, A.; Schneider, A.; Mihailetchi, V.D.; Koduvelikulathu, L.J.; Popescu, L.M.; Galbiati, G.; Chu, H.F.; Kopecek, R. Potential-induced degradation for encapsulated n-type IBC solar cells with front floating emitter. In Proceedings of the 5th International Conference on Silicon Photovoltaics, SiliconPV 2015, Konstanz, Germany, 25–27 March 2015; pp. 356–363.
19. Swanson, R.; Cudzinovic, M.; DeCeuster, D.; Desai, V.; Jürgens, J.; Kaminar, N.; Mulligan, W.; Rodrigues-Barbarosa, L.; Rose, D.; Smith, D. The surface polarization effect in high-efficiency silicon solar cells. In Proceedings of the 15th PVSEC, Shanghai, China, 10–15 October 2005.
20. Naumann, V.; Lausch, D.; Hahnel, A.; Bauer, J.; Breitenstein, O.; Graff, A.; Werner, M.; Swatek, S.; Grosser, S.; Bagdahn, J.; et al. Explanation of potential-induced degradation of the shunting type by Na decoration of stacking faults in Si solar cells. *Sol. Energy Mater. Sol. Cells* **2014**, *120*, 383–389. [CrossRef]
21. Oh, K.S.; Bae, S.; Lee, K.J.; Kim, D.; Chan, S.I. Mitigation of potential-induced degradation (PID) based on anti-reflection coating (ARC) structures of PERC solar cells. *Microelectron. Reliab.* **2019**, *100*, 113462. [CrossRef]
22. Masuda, A.; Akitomi, M.; Inoue, M.; Okuwaki, K.; Okugawa, A.; Ueno, K.; Yamazaki, T.; Hara, K. Microscopic aspects of potential-induced degradation phenomena and their recovery processes for p-type crystalline Si photovoltaic modules. *Curr. Appl. Phys.* **2016**, *16*, 1659–1665. [CrossRef]
23. Islam, M.A.; Hasanuzzaman, M.; Rahim, N.A. Investigation of the potential induced degradation of on-site aged polycrystalline PV modules operating in Malaysia. *Measurement* **2018**, *119*, 283–294. [CrossRef]
24. Wang, H.; Cheng, X.L.; Yang, H.; He, W.S.; Chen, Z.L.; Xu, L.H.; Song, D.Y. Potential-induced degradation: Recombination behavior, temperature coefficients and mismatch losses in crystalline silicon photovoltaic power plant. *Sol. Energy* **2019**, *188*, 258–264. [CrossRef]
25. Dupré, O.; Vaillon, R.; Green, M.A. Physics of the temperature coefficients of solar cells. Solar energy materials and solar cells. *Sol. Energy Mater. Sol. Cells* **2015**, *140*, 92–100. [CrossRef]
26. Dubey, R.; Batra, P.; Chattopadhyay, S.; Kottantharayil, A.; Arora, B.M.; Narasimhan, K.; Vasi, J. Measurement of temperature coefficient of photovoltaic modules in field and comparison with laboratory measurements. In Proceedings of the 2015 IEEE 42nd Photovoltaic Specialist Conference (PVSC), New Orleans, LA, USA, 14–19 June 2015; pp. 1–5.
27. Kaden, T.; Lammers, K.; Moller, H.J. Power loss prognosis from thermographic images of PID affected silicon solar modules. *Sol. Energy Mater. Sol. Cells* **2015**, *142*, 24–28. [CrossRef]
28. Mattei, M.; Notton, G.; Cristofari, C.; Muselli, M.; Poggi, P. Calculation of the polycrystalline PV module temperature using a simple method of energy balance. *Renew. Energy* **2006**, *31*, 553–567. [CrossRef]
29. Skoplaki, E.; Palyvos, J.A. On the temperature dependence of photovoltaic module electrical performance: A review of efficiency/power correlations. *Sol. Energy* **2009**, *83*, 614–624. [CrossRef]
30. King, D.L.; Kratochvil, J.A.; Boyson, W.E. Temperature coefficients for PV modules and arrays: Measurement methods, difficulties, and results. In Proceedings of the Conference Record of the Twenty Sixth IEEE Photovoltaic Specialists Conference-1997, Anaheim, CA, USA, 29 September–3 October 1997; pp. 1183–1186.
31. Evans, D.; Florschuetz, L. Terrestrial concentrating photovoltaic power system studies. *Sol. Energy* **1978**, *20*, 37–43. [CrossRef]
32. Segbefia, O.K.; Imenes, A.G.; Sætre, T.O. Outdoor Fault Diagnosis of Field-Aged Multicrystalline Silicon Solar Modules. In Proceedings of the 37th EU PVSEC, Lisbon, Portugal, 7–11 September 2020.
33. Segbefia, O.K.; Paudyal, B.R.; Burud, I.; Sætre, T.O. Temperature Coefficients of Photovoltaic Modules under Partial Shading Conditions. In Proceedings of the 38th EU PVSEC, Lisbon, Portugal, 6–10 September 2021; pp. 1180–1186.
34. Islam, M.A.; Hasanuzzaman, M.; Rahim, N.A. A comparative investigation on in-situ and laboratory standard test of the potential induced degradation of crystalline silicon photovoltaic modules. *Renew. Energy* **2018**, *127*, 102–113. [CrossRef]
35. Green, M.A. General temperature dependence of solar cell performance and implications for device modelling. *Prog. Photovolt. Res. Appl.* **2003**, *11*, 333–340. [CrossRef]
36. Buerhop, C.; Schlegel, D.; Niess, M.; Vodermayer, C.; Weigmann, R.; Brabec, C.J. Reliability of IR-imaging of PV-plants under operating conditions. *Sol. Energy Mater. Sol. Cells* **2012**, *107*, 154–164. [CrossRef]
37. Segbefia, O.K.; Imenes, A.G.; Burud, I.; Sætre, T.O. Temperature profiles of field-aged multicrystalline silicon photovoltaic modules affected by microcracks. In Proceedings of the 2021 IEEE 48th Photovoltaic Specialists Conference (PVSC), Fort Lauderdale, FL, USA, 20–25 June 2021; pp. 0001–0006.

38. Cheng, X.; Dong, Y.; Yang, T.; Zhou, T.; Wang, H.; Yu, H. Investigation on Temperature Coefficients of Crystalline Silicon Solar Modules before and after Potential-induced Degradation. In Proceedings of the 2019 IEEE 46th Photovoltaic Specialists Conference (PVSC), Chicago, IL, USA, 16–21 June 2019; pp. 1942–1945.
39. Spataru, S.; Hacke, P.; Sera, D.; Packard, C.; Kerekes, T.; Teodorescu, R. Temperature-dependency analysis and correction methods of in situ power-loss estimation for crystalline silicon modules undergoing potential-induced degradation stress testing. *Prog. Photovolt.* **2015**, *23*, 1536–1549. [CrossRef]
40. Green, M.; Emery, K.; Blakers, A. Silicon solar cells with reduced temperature sensitivity. *Electron. Lett.* **1982**, *18*, 97–98. [CrossRef]
41. Dupré, O.; Vaillon, R.; Green, M.A. Experimental assessment of temperature coefficient theories for silicon solar cells. *IEEE J. Photovolt.* **2015**, *6*, 56–60. [CrossRef]
42. Zhao, J.; Wang, A.; Robinson, S.; Green, M. Reduced temperature coefficients for recent high-performance silicon solar cells. *Prog. Photovolt. Res. Appl.* **1994**, *2*, 221–225. [CrossRef]
43. Reise, C.; Müller, B.; Moser, D.; Belluardo, G.; Ingenhoven, P. *Uncertainties in PV System Yield Predictions and Assessments*; IEA: Paris, France, 2018.
44. Berghold, J.; Koch, S.; Böttcher, A.; Ukar, A.; Leers, M.; Grunow, P. Potential-induced degradation (PID) and its correlation with experience in the field. *Photovolt. Int.* **2013**, *19*, 87–93.